MgII CGM Kinematics: Strong Dependencies with Galaxy Properties

Nikole M. Nielsen[1], Christopher W. Churchill[1], Glenn G. Kacprzak[2], Sebastian Trujillo-Gomez[1], Michael T. Murphy[2]

[1]New Mexico State University, [2]Swinburne University of Technology

astronomy.nmsu.edu/cwc/Group/magiicat

Introduction & Motivation

The MgII $\lambda\lambda$2796, 2803 doublet is ideal for studying the CGM as it samples galaxies over the redshift range where they can be studied in detail. MgII is observed in outflowing winds (e.g., Weiner et al. 2009) and infalling accretion (e.g., Rubin et al. 2012) and trends have been reported between MgII and star formation rate, L_B/L_B^*, and/or stellar mass of the host galaxy (e.g., Chen et al. 2010; Ménard et al. 2011). Gas is preferentially located along the galaxy's minor or major axis (e.g., Kacprzak et al. 2012), suggesting bipolar outflowing winds and coplanar accretion are the dominant structures traced by MgII.

To further our understanding of the galaxy-CGM connection, a kinematic study of the gas around galaxies and how the gas responds to the galaxy is an important step to understanding galaxy evolution.

MgII Absorber-Galaxy Catalog (MAGIICAT)

- 182 absorber-galaxy pairs with detected or upper limit on MgII absorption
- Spectroscopic redshifts: $0.07 < z_{gal} < 1.1$
- Quasar-galaxy impact parameters: $D < 200$ kpc
- *B*- and *K*-band luminosities and *B-K* colors
- Halo masses, M_h, from halo abundance matching (e.g., Trujillo-Gomez 2011)
- Virial radii, R_{vir}, from M_h
- *HIRES/UVES data for 48 MgII absorbing galaxies – results from this subset of MAGIICAT galaxies are presented in the center and right columns*

Papers using MAGIICAT data:

Paper I: Nielsen+ 2013, ApJ, 776, 114
Paper II: Nielsen+ 2013, ApJ, 776, 115
Paper III: Churchill+ 2013, ApJ, 779, 87
Paper IV: Nielsen+ 2014, ApJ, in prep
CGM/Halo Mass: Churchill+ 2013, ApJ, 763, L42
CGM/Orientation: Kacprzak+ 2012, ApJ, 760, L7

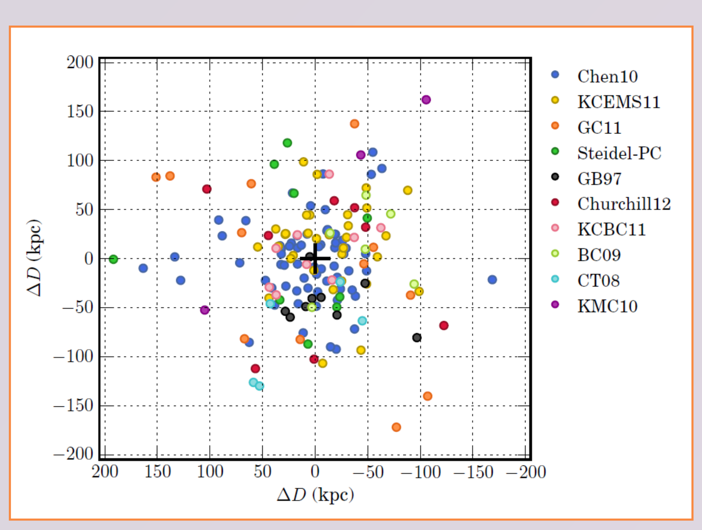

Figure 1 – Galaxy Offsets from the Background Quasars
Offsets in physical units of each galaxy having measurements of $\Delta\alpha$ and $\Delta\delta$ from the associated background quasar (plus sign). Points are colored by the work from which the galaxy was obtained.

$W_r(2796)$ is anti-correlated with D at the 7.9σ level - the quantity and covering fraction of halo gas diminishes with projected distance.

A log-linear fit, $\log W_r(2796) = \alpha_1 D + \alpha_2$, is the best parameterization of the data, with $\alpha_1 = -0.015\pm0.002$ and $\alpha_2 = 0.27\pm0.11$.

Mass dependence: at a given D, higher mass halos have larger absorption equivalent widths (Churchill et al. 2013a,b). This implies self-similarity in the cool/warm CGM.

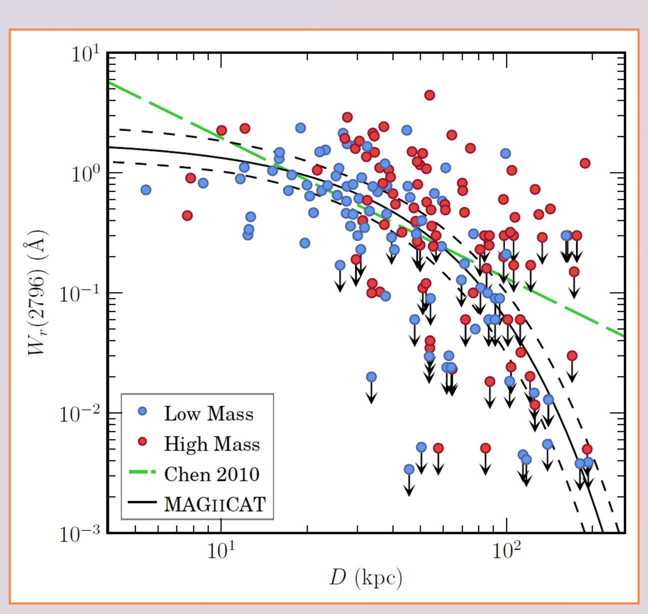

Figure 2 – $W_r(2796)$ vs D Sliced by Halo Mass
The dashed green line is the log-log fit to the data presented in Chen et al. (2010). The solid black line is a log-linear maximum likelihood fit to the data.

MgII Absorption Profiles

Figure 3 presents the $W_r(2796)$ absorption profiles as a function of D for 48 galaxies in which MgII was detected in HIRES/UVES spectra. The gas kinematics were modeled using Voigt profile fits (Evans 2011) and are presented as red profiles.

Clouds per Halo & Cloud Velocities

Absorption at larger impact parameters from the host galaxy may have a larger number of clouds per halo than at smaller impact parameters in terms of the mean (t-test), dispersion (f-test), and general distribution of data (Kolmogorov-Smirnov test).

Higher L_B/L_B^* galaxies may have a larger spread in the number of clouds per halo than lower L_B/L_B^* galaxies.

Subsample Cut	Statistical Test	Significance
D = 37.7 kpc	t-test	2.3σ
	f-test	2.4σ
	KS test	2.6σ
L_B/L_B^* = 0.52	f-test	2.5σ

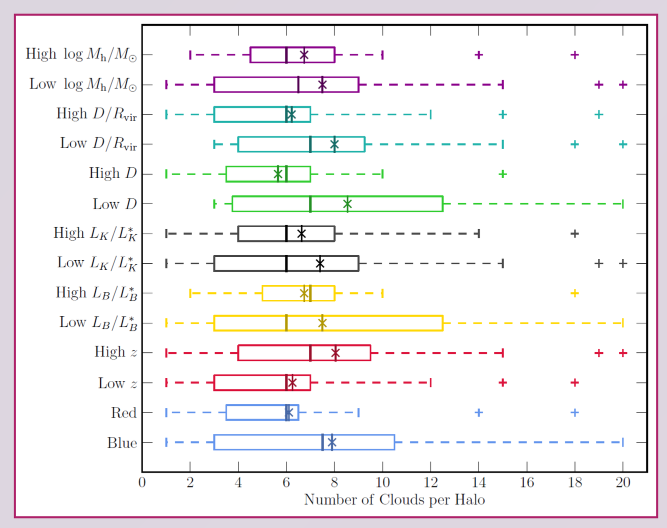

Figure 4 – Number of Clouds per Halo
For each galaxy subsample, the median number of clouds per halo is denoted by the vertical line in each box and the mean number by the vertical line with an x . The range of each horizontal box indicates the inner 50% data range and the ranges of the dashed, capped lines show the outer 50%, excluding outlier points. The plusses indicate outliers.

Most absorption is not escaping the host galaxy, even at the virial radius. For the absorption that is escaping, it tends to be hosted by redder galaxies and lower mass galaxies. At a given mass, redder galaxies may have larger velocities than bluer galaxies.

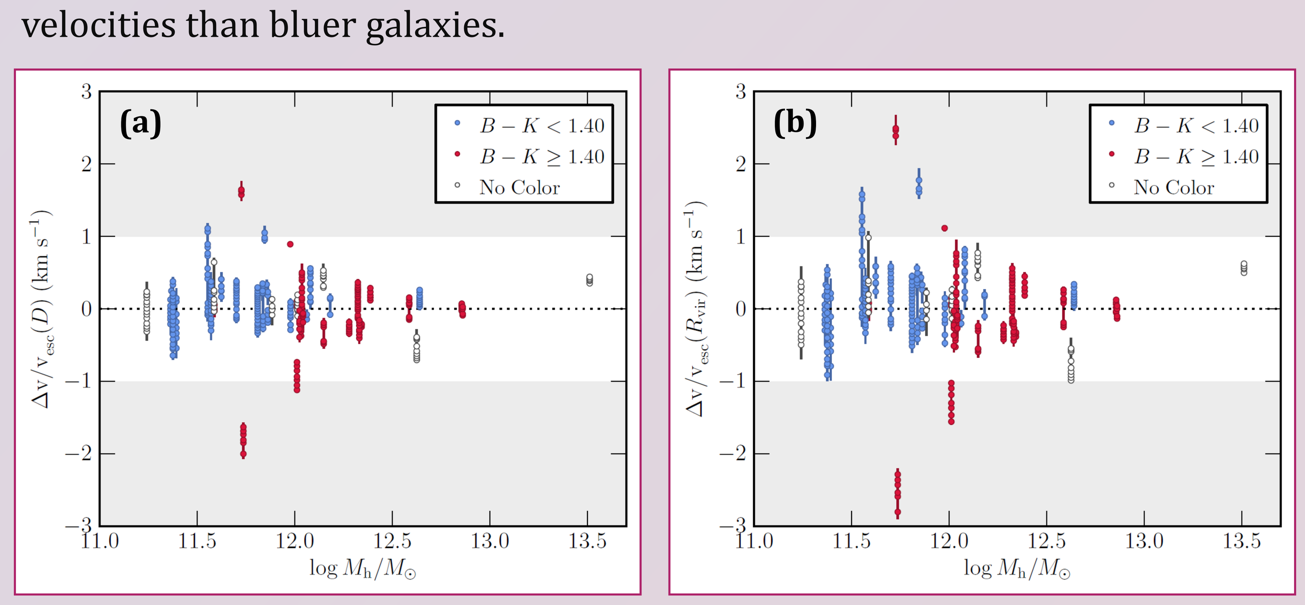

Figure 5 – Cloud Velocities Normalized by v_{esc} vs Halo Mass
(a) The escape velocity, v_{esc}, calculated at *D*, the minimum distance the absorbing material could be located from the galaxy. (b) v_{esc} calculated at R_{vir}. Points indicate individual clouds from VP modeling and the vertical lines show the velocity range for each absorber, both colored by *B-K*. Absorbers in shaded regions are likely escaping their host galaxies.

Column Density Distributions

The slopes for high and low mass (and high and low L_K/L^*_K) are not consistent within uncertainties; high mass galaxies have more smaller column density clouds and low mass galaxies have more larger column density clouds.

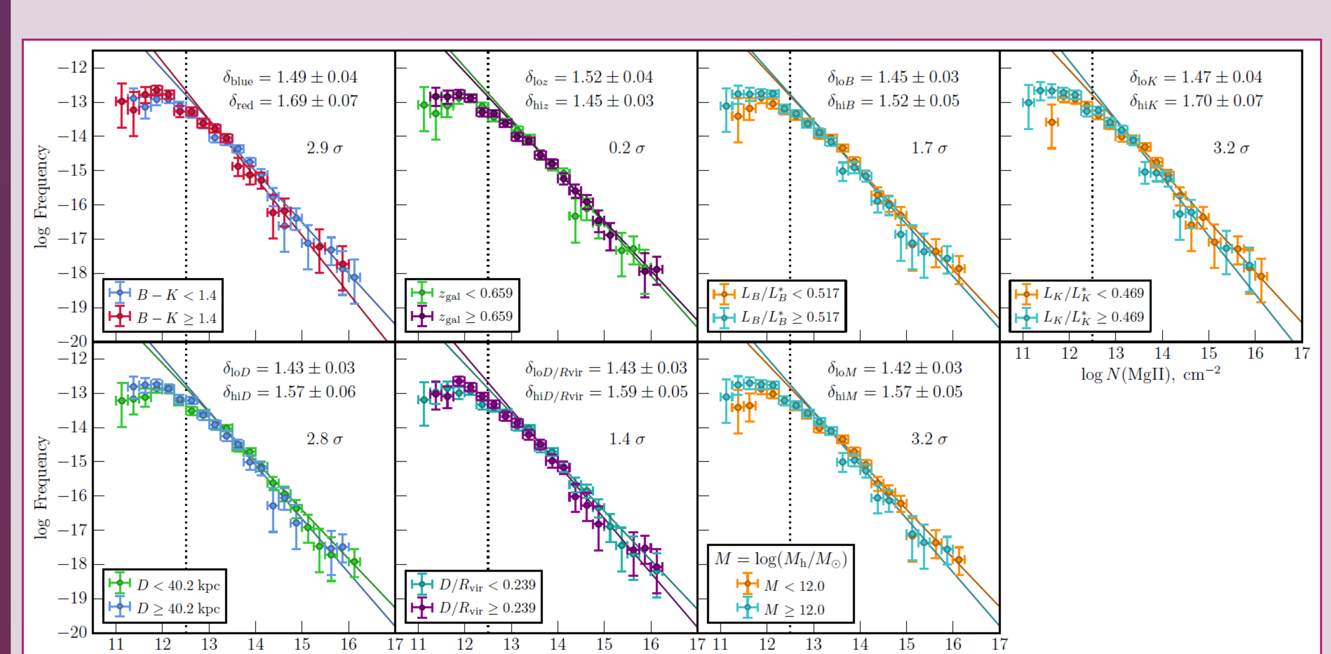

Figure 6 – Column Density Distributions, *f(N)*, for Galaxy Subsamples
Points represent binned column densities, the dotted line indicates a completeness limit of $\log N$(MgII) = 12.5, and the solid lines are maximum likelihood fits to the unbinned data above the completeness limit. The slopes of the fits and the significance of a KS test between subsamples are located in the upper right of each panel.

Cloud-Cloud Velocity Clustering

The two-point velocity correlation function (TPCF) is the probability of finding any two clouds separated by a particular velocity difference, Δv. In every case, statistical tests (Chi-square test, f-test and Kolmogorov-Smirnov) between two subsamples show that the TPCFs are not drawn from the same population at greater than 10σ.

Figure 7 – TPCFs for Various Subsamples Split by Galaxy Properties
Solid lines are the TPCF while the shading around the solid line represents the 1σ Poisson uncertainties.

(left) Un-normalized, Δv **(right) Normalized, $\Delta v/V_{circ}$**

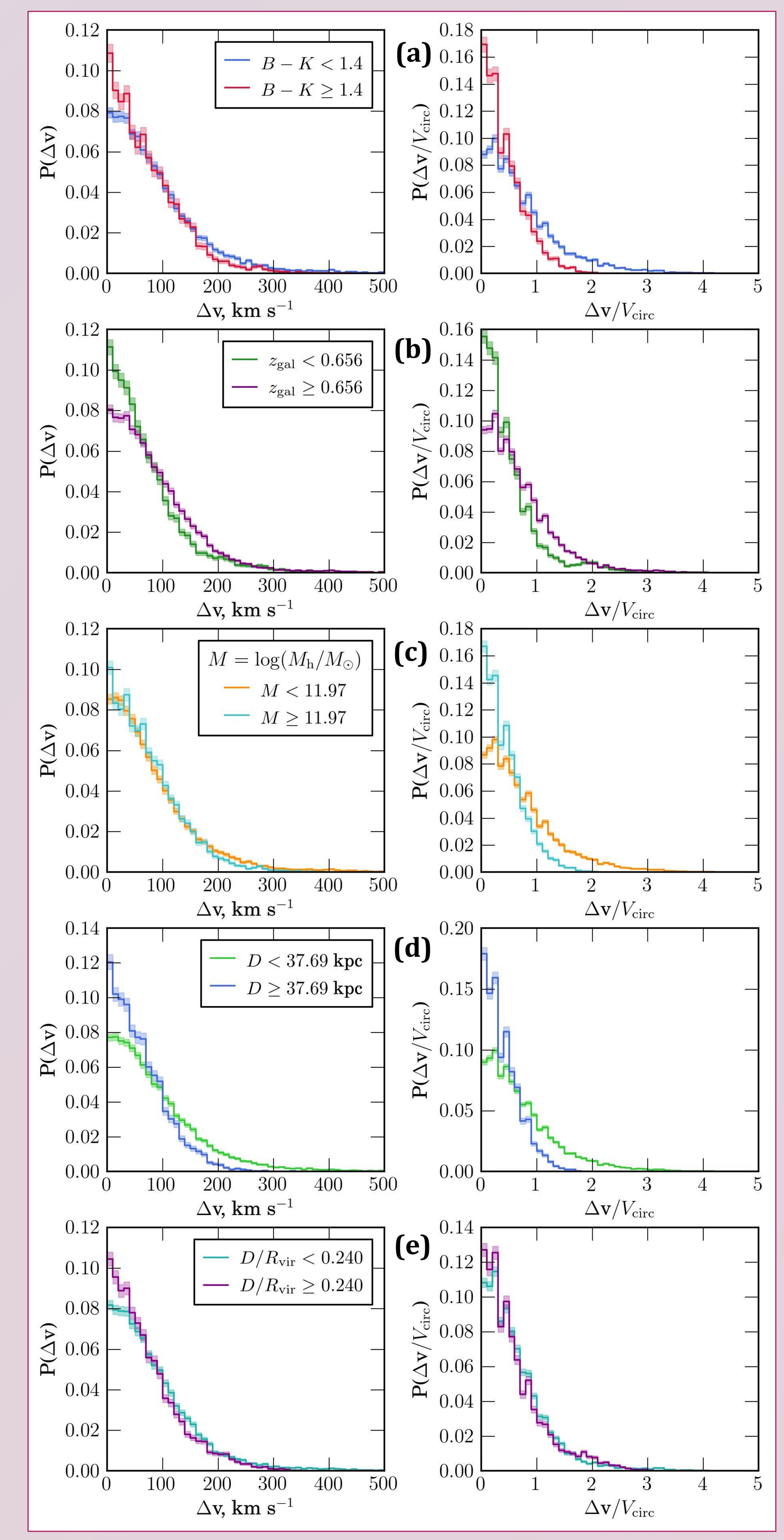

Panel (a): Rest-frame *B-K* color

Panel (b): Galaxy redshift, z_{gal}

Panel (c): Halo mass, M_h

Panel (d): Impact parameter, *D*

Panel (e): Impact parameter normalized by the galaxy virial radius, D/R_{vir}

Conclusions

- The MgII CGM depends strongly on the host galaxy's mass and where the galaxy is being probed with respect to the virial radius, suggesting self-similarity.
- The number of clouds, and cloud column densities and velocities depend strongly on the type of galaxy the absorption lives in and where in the CGM.
- Studying the CGM of galaxies with absorption in background quasars is only useful if information is known about the host galaxy properties.

References

Chen, H.-W., Helsby, J. E., Gauthier, J.-R., et al. 2010, ApJ, 714, 1521
Churchill, C. W., Nielsen, N. M., Kacprzak, G. G., & Trujillo-Gomez, S. 2013a, ApJ, 763, L42
Churchill, C. W., Trujillo-Gomez, S., Nielsen, N. M., & Kacprzak, G. G. 2013b, ApJ, 779, 87
Evans, J. L. 2011 Ph.D. Thesis, New Mexico State University
Kacprzak, G. G., Churchill, C. W., & Nielsen, N. M. 2012, ApJ, 760, L7
Ménard, B., et al. 2011, MNRAS, 417, 801M
Nielsen, N. M., Churchill, C. W., & Kacprzak, G. G. 2013, ApJ, 776, 115 (Paper II)
Nielsen, N. M., Churchill, C. W., Kacprzak, G. G., & Murphy, M. T. 2013, ApJ, 776, 114 (Paper I)
Rubin, K. H. R., Prochaska, J. X., Koo, D. C., & Phillips, A. C. 2012, ApJ, 747L, 26R
Trujillo-Gomez, S., Klypin, A., Primack, J., & Romanowsky, A. J. 2011, ApJ, 742, 16
Weiner, B. J., et al. 2009, ApJ, 692, 187W

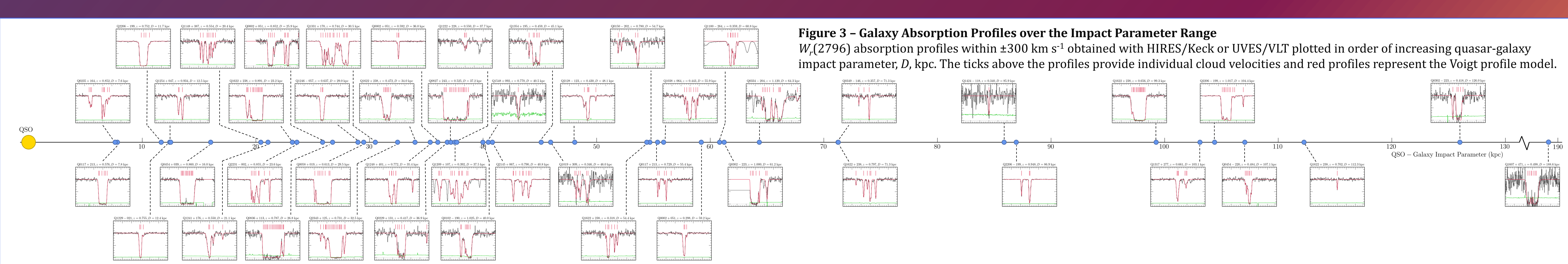

Figure 3 – Galaxy Absorption Profiles over the Impact Parameter Range
$W_r(2796)$ absorption profiles within ±300 km s^{-1} obtained with HIRES/Keck or UVES/VLT plotted in order of increasing quasar-galaxy impact parameter, *D*, kpc. The ticks above the profiles provide individual cloud velocities and red profiles represent the Voigt profile model.